Bioconjugate Chemistry

Subscriber access provided by CORNELL UNIVERSITY LIBRARY

Article

Fabrication of Polymeric Micelles with AIE and FRET for Anticancer Drug Delivery

Na Hao, Changzhen Sun, Zhengfei Wu, Long Xu, Wenxia Gao, Jun Cao, Li Li, and Bin He

Bioconjugate Chem., **Just Accepted Manuscript** • Publication Date (Web): 01 Jun 2017

Downloaded from http://pubs.acs.org on June 2, 2017

Just Accepted

"Just Accepted" manuscripts have been peer-reviewed and accepted for publication. They are posted online prior to technical editing, formatting for publication and author proofing. The American Chemical Society provides "Just Accepted" as a free service to the research community to expedite the dissemination of scientific material as soon as possible after acceptance. "Just Accepted" manuscripts appear in full in PDF format accompanied by an HTML abstract. "Just Accepted" manuscripts have been fully peer reviewed, but should not be considered the official version of record. They are accessible to all readers and citable by the Digital Object Identifier (DOI®). "Just Accepted" is an optional service offered to authors. Therefore, the "Just Accepted" Web site may not include all articles that will be published in the journal. After a manuscript is technically edited and formatted, it will be removed from the "Just Accepted" Web site and published as an ASAP article. Note that technical editing may introduce minor changes to the manuscript text and/or graphics which could affect content, and all legal disclaimers and ethical guidelines that apply to the journal pertain. ACS cannot be held responsible for errors or consequences arising from the use of information contained in these "Just Accepted" manuscripts.

ACS Publications

Bioconjugate Chemistry is published by the American Chemical Society. 1155 Sixteenth Street N.W., Washington, DC 20036

Published by American Chemical Society. Copyright © American Chemical Society. However, no copyright claim is made to original U.S. Government works, or works produced by employees of any Commonwealth realm Crown government in the course of their duties.

Fabrication of Polymeric Micelles with AIE and FRET for Anticancer Drug Delivery

Na Hao,[a] Changzhen Sun,[a] Zhengfei Wu,[a] Long Xu,[a] Wenxia Gao,[b] Jun Cao,[a] Li Li [a]*, Bin He [a]*

[a] National Engineering Research Center for Biomaterials, Sichuan University, Chengdu 610064, China

[b] College of Chemistry and Materials Engineering, Wenzhou University, Wenzhou 325027, China

Corresponding authors:

Wenxia Gao

Tel/Fax:+86-577-88368280

Email: wenxiag@wzu.edu.cn

Li Li

Tel: +86-28-8547 0770

Fax: +86-28-8541 2848

Email: li_li@scu.edu.cn

ABSTRACT

With the aim to obtain effective cancer therapy of simultaneous cellular imaging, dynamic drug release monitoring and chemotherapeutic treatment, a polymeric micelle with aggregation-induced emission (AIE) imaging and forster resonance energy transfer (FRET) effect was fabricated as the drug carrier. Amphiphilic conjugate of MAL-PEG-Tripp bearing AIE molecules were synthesized and self-assembled into micelles to load anticancer drug doxorubicin (DOX). Spherical DOX-loaded micelles with the mean size of 106 nm were obtained with good physiological stability (CMC, 12.5 μg/mL), high drug loading capacity (10.4%) and encapsulation efficiency (86%). The cellular uptake behavior of DOX-loaded MAL-PEG-Tripp micelles was visible for high-quality intracellular imaging due to the AIE property. The delivery of DOX from the drug-loaded micelles was dynamic monitored by the FRET effect between the DOX and MAL-PEG-Tripp. Both in vitro (IC50, 2.36 μg/mL) and in vivo anticancer activity tests revealed that the DOX-loaded MAL-PEG-Tripp micelles exhibited promising therapeutic efficacy to cancer with low systematic toxicity. In summary, this micelle provided an effective way to fabricate novel nanoplatform for intracellular imaging, drug delivery tracing and chemotherapy.

KEYWORDS

polymeric micelle, AIE imaging, FRET effect, chemotherapy

INTRODUCTION

Multifunctional nanocarrier has attracted more and more attention for its effective cancer therapeutic effect.[1,2] The theranostic nanoparticles integrated with diagnostic imaging and therapeutic capability have exhibited great potential for tumor therapy by realizing imaging-guided drug delivery and tumor treatment.[3-5] In order to obtain the imaging guider, intracellular tracing nanomedicine based on fluorescent tagging has became an important method.[6-8] Conventional fluoresent dyes such as fluorescein isothiocyanate (FITC), rhodamine and quantum dots are commonly used as fluorescent imaging materials.[9-11] However, the drawbacks such as instability in modification, hydrolysis and detachment of dyes during the phagocytic process impede the performance for bioimaging.[12] Quantum dots based biosensors and fluoresent inorganic dyes have relatively strong and stable fluorescence, they suffer from the toxicity to the cell due to their nonbiodegradation and intrinsic heavy metal toxicity.[13-15] Moreover, traditional fluorogens further suffer from aggregation caused quenching (ACQ) when incorporated in nanoparticles with high loading content, which greatly reduces the fluorescence intensity and impedes the imaging effect.[16-17] Therefore, the novel category of fluorophores with aggregation induced emission (AIE) effect has attracted great interest since it was reported in 2001.[18-19] The AIE probes have been employed for cell imaging.[20-23] The nano-aggregates can stay inside the live cells for long time without fluorescence reduction to enable long-term cell tracing for the whole biological event.[24-26] Taking advantage of this unique AIE property, we fabricated an AIE-active polymeric micelle as drug carrier with the fluorescent imaging in this study.

Although the cellular uptake of polymeric micelles could be intracellular traced by the AIE effect in the nano-drug carrier, the drug release behavior of the nanoparticles is still unknown. With the expectation to investigate the intracellular drug release from nanoparticles, we further introduce the forster resonance energy transfer (FRET) effect between the AIE group and antitumor drug of doxorubicin (DOX) as FRET is a dynamic process monitoring for specific imaging systems.[27-29] In this study, we use the molecular interaction between the AIE group and DOX to detect drug release using the mechanism that the FRET effect between the AIE group and DOX would disappear when DOX was released from nanoparticles. A polymeric micelle with the capacity for simultaneous cellular imaging, dynamic drug release monitoring, and chemotherapy was fabricated for effective cancer therapy (Figure 1) .

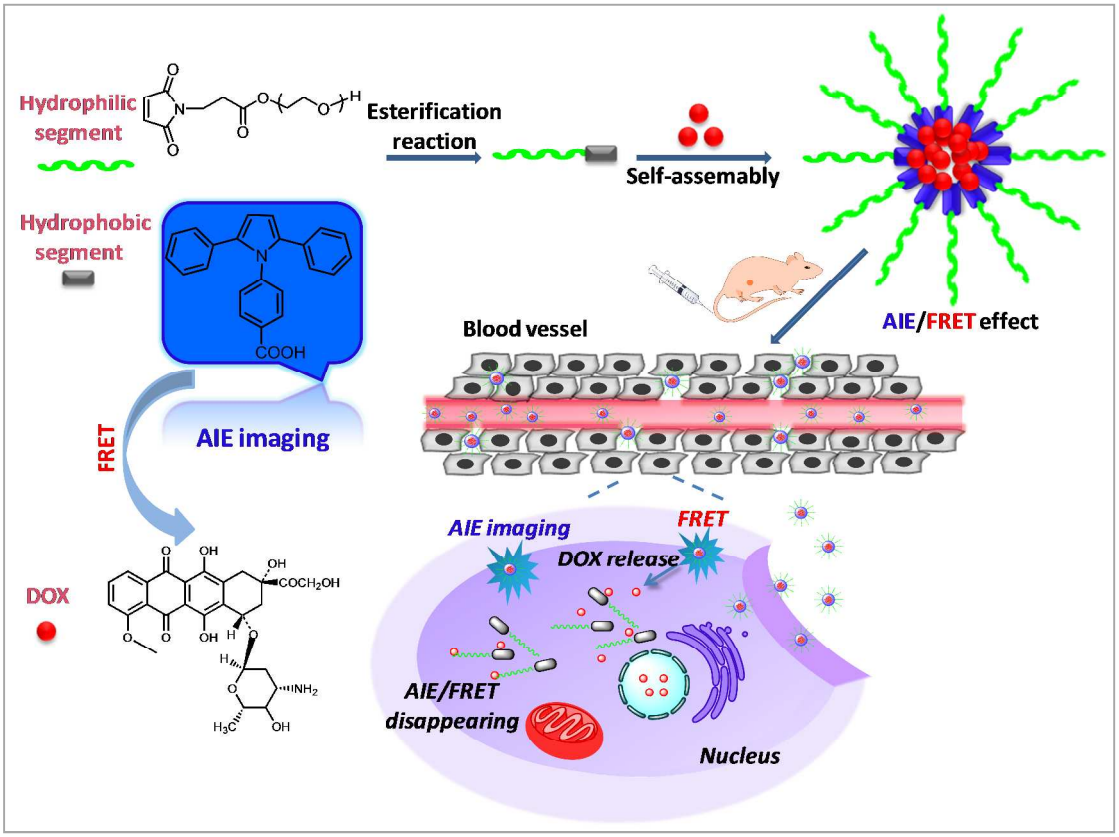

Figure 1. Schematic diagram of the self-assembly of polymeric micelles with AIE imaging and FRET effect for anticancer drug delivery.

RESULTS AND DISCUSSION

Preparation and characterization of polymeric micelles

This study aimed to fabricate a novel polymeric micelles with AIE effect for cell imaging and FRET effect for monitoring anticancer drug delivery of doxorubicin (Figure 1). We expected that the synthetic polymer molecule could self-assemble into micelles in which the hydrophobic AIE molecule core was used not only for cell imaging but also for loading hydrophobic anticancer drugs, and the hydrophilic PEG moiety could serve as a micelle shell with a long blood circulation time. The amphiphile of MAL-PEG-Tripp was designed and synthesized as shown in Scheme 1. The ^{1}H NMR spectra of Tripp-COOH and MAL-PEG-Tripp were shown in Figure 2. The chemical shifts of the protons in Tripp-COOH were located at 6.50 ppm (1), 7.03 -7.24 ppm (2-5), 7.85 ppm (6), 13.12 ppm (7), respectively. As for MAL-PEG-Tripp, except for the characteristic chemical shifts of Tripp-COOH, the peaks at 3.30-3.81 ppm (8, 10) were assigned to the protons of OCH_2CH_2 in PEG, and the other two protons of $COCH_2CH_2$ and CH_2CH_2N in 1H-Pyrrole-1-propanoicacid were appeared at 2.40-2.60 ppm

(11), and 4.61 ppm (12), respectively. The peak at 13.12 ppm assigned to the terminal carboxyl disappeared after esterification. The conjugate was further confirmed by molecular weight of MALDI-TOF-MS analysis (Figure S1), the molecular weight of MAL-PEG was right-shifted after conjugation.

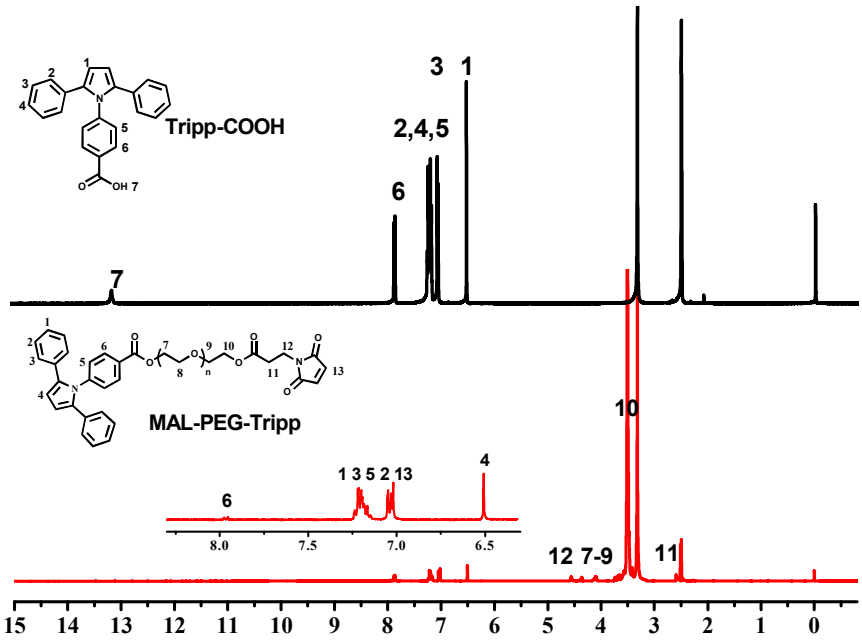

Figure 2. The ^{1}H NMR spectra of Tripp-COOH and MAL-PEG-Tripp with DMSO-d_6 as solvent.

The size distribution and morphology of the micelles were tested by DLS and SEM. Both blank and DOX-loaded MAL-PEG-Tripp micelles were well dispersed in aqueous media. The mean size of blank MAL-PEG-Tripp micelles was about 91 nm (Figure 3A) and that of DOX-loaded MAL-PEG-Tripp micelles was about 106 nm (Figure 3B). Both blank and drug-loaded micelles were spherical in SEM images and the size was consistent with DLS result. The relative small mean size was highly suitable for nanoparticles to evade scavenging by the mononuclear phagocyte system (MPS) and passive targeting via enhanced permeability and retention (EPR) effect.[30] The critical aggregation concentration (CMC) for the micelles was also investigated to evaluate the stability of micelles. Since the amphiphiles of MAL-PEG-Tripp possessed the AIE property when they self-assembled into micelles in aqueous solution, here we used this mechanism to test the CMC of micelles, the tested CMC was 12.5 μg/mL (Figure S2). It implied that the MAL-PEG-Tripp micelles were very stable when highly diluted, which was necessary for intravenous application. Furthermore, the DOX-loaded MAL-PEG-Tripp micelles had high drug-loading capacity (DLC) of 10.4% and high drug encapsulation efficiency (DEE) of 86%.

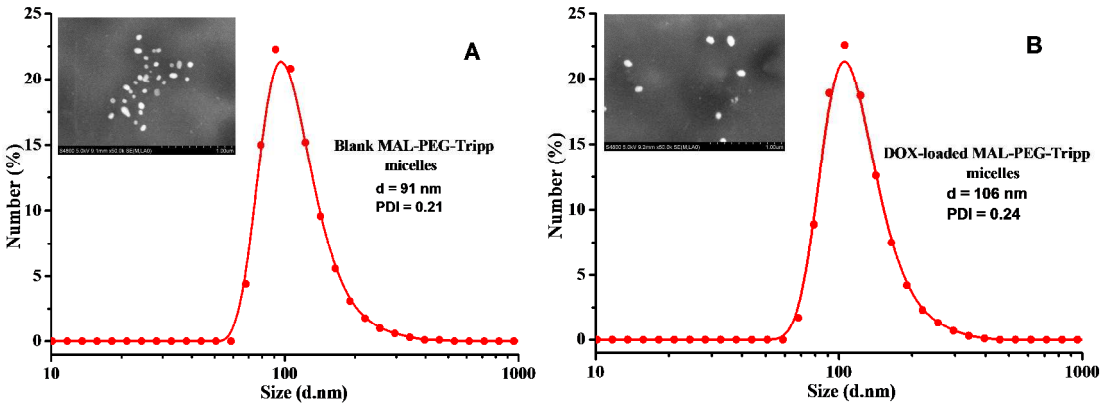

Figure 3. DLS and SEM images of (A) blank MAL-PEG-Tripp micelles and (B) DOX-loaded MAL-PEG-Tripp micelles micelle.

AIE imaging and FRET effect of the micelles

Since the Tripp-COOH groups as the hydrophobic moieties in the amphiphile MAL-PEG-Tripp were trapped into the micellar cores during the micellar formation, the aggregation state of Tripp-COOH molecules would excite the AIE behavior. The AIE behavior of MAL-PEG-Tripp could be evaluated by fluorescence assay. With the same concentration and excitation condition, MAL-PEG-Tripp dissolved in DMSO showed weak fluorescent, the fluorescent intensity increased dramatically with adding water to the DMSO solution (Figure 4A). Interestingly, when the water fraction (*f*w) reached 99 vol%, the fluorescent intensity of MAL-PEG-Tripp in water was nearly 52-fold stronger than that in 100% DMSO (Figure 4B). This result indicated the AIE effect of MAL-PEG-Tripp micelles, which was further used for cell imaging.

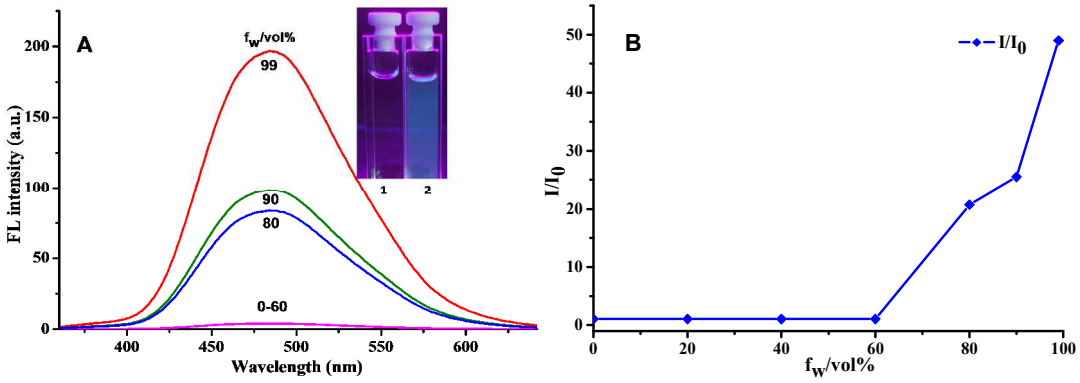

Figure 4. The fluorescent spectra of micelles, (A) fluorescent spectra of MAL-PEG-Tripp in DMSO/water mixtures with different fractions of water (*f*w), insert image showing fluorescence of MAL-PEG-Tripp solutions dissolved in pure DMSO (1) and 99% water (2); (B) plot of fluorescent intensity of MAL-PEG-Tripp versus

water content of DMSO/water mixture, I= fluorescent intensity of MAL-PEG-Tripp in mixed solution, I_0 = fluorescent intensity of MAL-PEG-Tripp in pure DMSO (λex= 330 nm).

Besides the AIE effect of the MAL-PEG-Tripp micelles, DOX-loaded MAL-PEG-Tripp micelles also showed FRET effect. A phenomenon was found when blank MAL-PEG-Tripp micelles and DOX-loaded MAL-PEG-Tripp micelles were excited at the same wavelength of 330 nm. Two emission peaks were obtained for the DOX-loaded MAL-PEG-Tripp micelles excited at 330 nm, one was around 470 nm assigned to the Tripp group in blank MAL-PEG-Tripp micelles, and the other around 580 nm was assigned to DOX (Figure 5A). This result demonstrated the Tripp group was firstly excited at 330 nm and gave the emission wavelength of 470 nm, The emission of 470 nm was further acted as the excitation wavelength for DOX, which demonstrated the FRET effect occurred between Tripp and DOX. This phenomenon was further explained by the absorption and emission spectra of MAL-PEG-Tripp and DOX (Figure 5B). The existence of FRET phenomenon might also be related to the π-π stacking between DOX and the AIE group of Tripp (Figure S3), a significant fluorescence quenching and red shift in UV spectra occurred when the DOX was encapsulated in the micelles .

The FRET phenomenon was further used to keep tracking drug release process of DOX from the micelles. The DOX release profiles of the DOX-loaded MAL-PEG-Tripp micelles at different pH were investigated (Figure 5C). The amounts of released DOX at different predetermined time points were measured by fluorescence detector (λex= 480 nm, λem= 550 nm). The curves exhibited a biphasic pattern including an early burst release and followed sustaining release. The burst release was the rapid transfer of DOX adsorbed to the surface of micelles, and the sustaining release was the diffusion of DOX from micellar cores. The accumulated release rates of DOX-loaded MAL-PEG-Tripp micelles was about 28% at pH 7.4 and 67% at pH 5.5 in the first 24 h, respectively. And finally the drug release from DOX-loaded MAL-PEG-Tripp micelles was much higher at pH 5.5 (90%) than that at pH 7.4 (35%). The DOX-loaded MAL-PEG-Tripp micelles exhibited faster release in lower pH environment such as in lysosomes. During the process of drug release, the fluorescence of DOX-loaded MAL-PEG-Tripp micelles was detected (Figure 5D). The progressive decline in emission at wavelength of 500 nm-700 nm (emission of acceptor DOX) was in accompany with the gradually growth in emission at wavelength of 470 nm (emission of donor MAL-PEG-Tripp) with the extension of release time. This result demonstrated the FRET effect between the DOX and MAL-PEG-Tripp was weakened gradually till it disappeared with the release of DOX from the drug loaded micelles. The delivery of DOX could be dynamic monitored by the FRET effect.

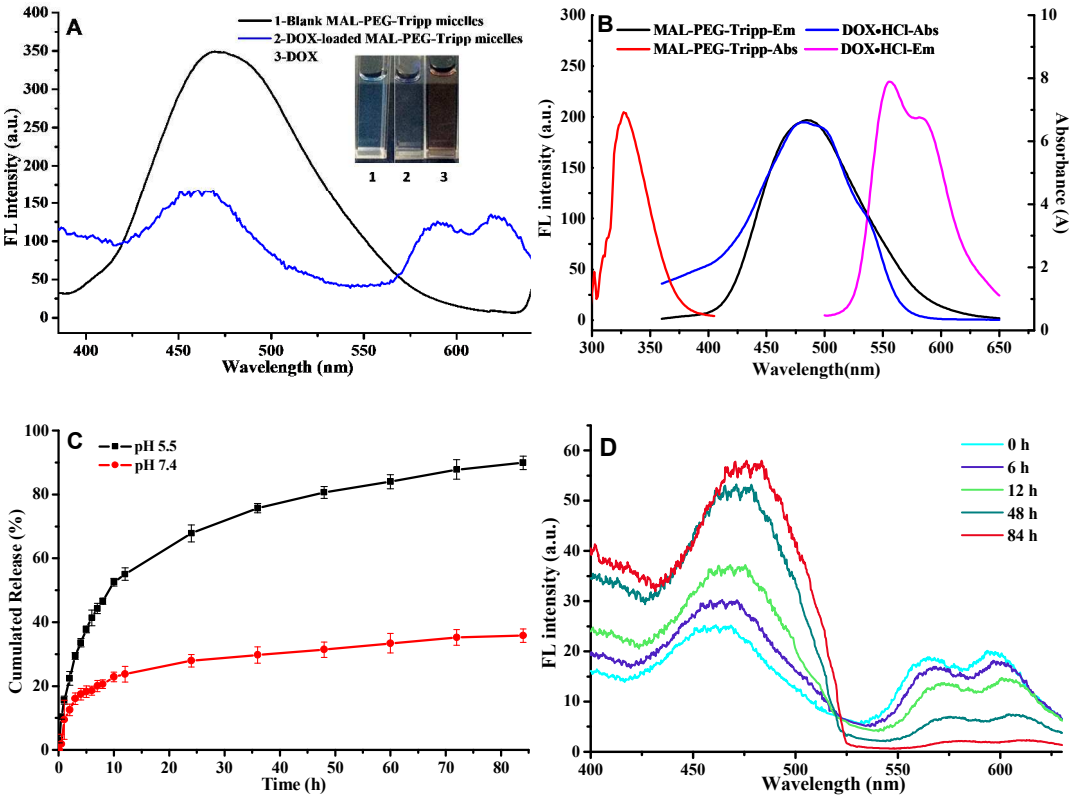

Figure 5. Fluorescence spectra of blank micelles and DOX-loaded MAL-PEG-Tripp micelles (λex= 330 nm), inset: photograph showing fluorescence of blank micelles (1), DOX-loaded micelles (2), and DOX (3) under UV irradiation at 365 nm (A); the absorption and emission spectra of MAL-PEG-Tripp and DOX (B); the release profiles of DOX-loaded MAL-PEG-Tripp micelles at pH 5.5 and 7.4, means ± SD (n =3) (C); the fluorescence spectra of DOX-loaded MAL-PEG-Tripp micelles in PBS (pH 5.5) at different time during DOX releasing (λex= 330 nm) (D).

Stability of DOX-loaded micelles

Furthermore, the stability of DOX-loaded MAL-PEG-Tripp micelles was examined in serum-supplemented medium by monitoring the change of MAL-PEG-Tripp and DOX fluorescent intensity. If the fluorescent intensity of MAL-PEG-Tripp decreased or disappeared, it indicated that the DOX-loaded MAL-PEG-Tripp micelles disassembled. Alternatively, once DOX released from DOX-loaded MAL-PEG-Tripp micelles, the fluorescence intensity of DOX would increase because it was not affected by the ACQ effect and the fluorescence intensity of the MAL-PEG-Tripp would also increase as the emission from MAL-PEG-Tripp was no longer transferred to DOX via FRET. As shown in Figure S4, after incubated with serum for 24 h, the fluorescence intensity of MAL-PEG-Tripp was almost not changed and the fluorescence intensity of DOX was

slightly enhanced, we considered that this might be due to a small amount of DOX release from the DOX- loaded micelle. The results illustrated that DOX-loaded MAL-PEG-Tripp micelles were stable in serum.

In vitro anticancer activity study

The cytotoxicity of blank MAL-PEG-Tripp micelle was evaluated with 4T1 breast cancer cells and C2C12 cells via CCK-8 assay (Figure S5). The result indicated that the micelles were non-toxic after incubated for 48 h even when the concentration increased to 1mg/mL. The DOX-loaded MAL-PEG-Tripp micelles were incubated with 4T1 cells at different drug concentrations to study the in vitro anticancer activities. The intracellular localization and distribution of DOX-loaded MAL-PEG-Tripp micelles were investigated using confocal fluorescence microscopy (CLSM). As shown in Figure 6, the blue fluorescence of both blank and DOX-loaded MAL-PEG-Tripp micelles were all clearly observed in the cytoplasm, which indicated the accumulation of MAL-PEG-Tripp molecules in the cytoplasm. In the images of DOX•HCl samples, red fluorescence was observed in both cytoplasm and nuclei, it was attributed to the excellent solubility of DOX•HCl in aqueous medium, DOX•HCl was internalized in the cells and rapidly reached nuclei via passive diffusion mechanism. However, for the DOX-loaded MAL-PEG-Tripp micelles, most of the red fluorescence of DOX was concentrated in cytoplasm, only weak read fluorescence was observed in nuclei. The fluorescence intensity of both DOX and MAL-PEG-Tripp increased for 3 h incubation comparing to 1 h incubation, which implied that more drug loaded micelles were internalized into cells and a sustained release of DOX from the DOX-loaded MAL-PEG-Tripp micelles was happened. This result demonstrated that the DOX-loaded MAL-PEG-Tripp micelles could be internalized through an endocytosis process.

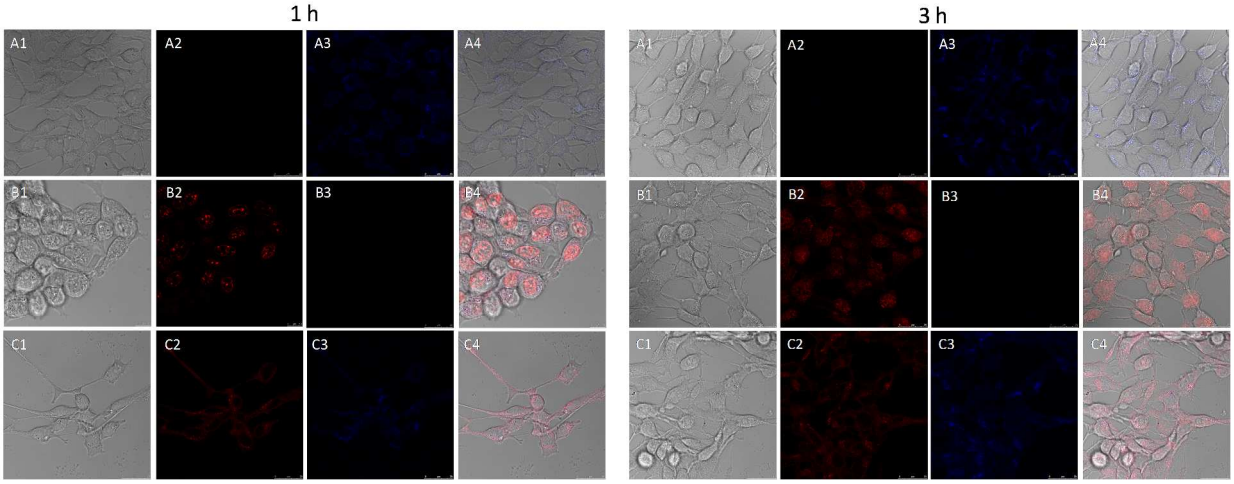

Figure 6. The confocal laser scanning microscopy images of 4T1 cells incubated with blank MAL-PEG-Tripp micelles (A), DOX•HCl (B), and DOX-loaded MAL-PEG-Tripp micelles (C) for 1 h and 3 h, the 1, 2, 3 and 4

represented the images of bright field, fluorescence channel of DOX, MAL-PEG-Tripp, and overlay, the scale bar was 20 mm.

In order to further investigate the intracellular distribution of the micelles after cellular uptake, staining of lysosomes with Lysotracker Green was observed by CLSM. As shown in Figure 7, the blue fluorescence from blank MAL-PEG-Tripp micelles and DOX-loaded MAL-PEG-Tripp micelles was mostly co-localized with the green fluorescence of lysosomes, which indicated that MAL-PEG-Tripp remained in the cytoplasm as luminescent micelles. Meanwhile, for DOX loaded micelles-treated cells, we found that the strong red fluorescence signal was observed in the cytoplasm and weak red fluorescence was observed in the cell nucleus, this indicated that most of the DOX was still in the lysosomes and only a small amount of DOX was delivered into cells nucleus.

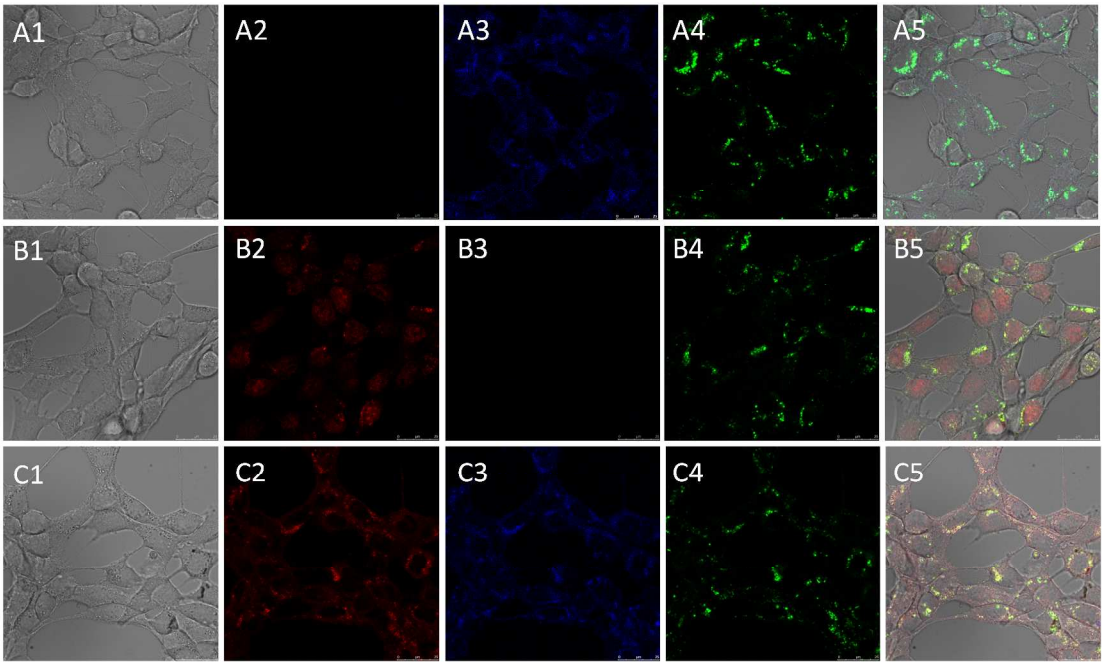

Figure 7. The confocal laser scanning microscopy images of spatiotemporal distributions of blank MAL-PEG-Tripp micelles (A), DOX (B), and DOX-loaded MAL-PEG-Tripp micelles (C) co-localized with lysosomes in 4T1 cells for 3 h, the 1, 2, 3, 4 and 5 represented the images of bright field, fluorescence channel of DOX, MAL-PEG-Tripp, Lysotracker Green and overlay, the scale bar was 20 mm.

To investigate the existence of FRET phenomenon in the cell, the images of CLSM were taken by using three separate channels to collect the emission of MAL-PEG-Tripp (donor), DOX (acceptor) and FRET channel. A 405 nm laser was used to excite the MAL-PEG-Tripp in the donor channel and the emission was collected from

475 to 495 nm (blue fluorescence). The acceptor channel was excited at 488 nm for the DOX and the emission was collected from 550 to 625 nm (red fluorescence). The FRET channel was excited at 405 nm for the MAL-PEG-Tripp donor, and the emission of DOX excited by energy transfer from donor was also collected from 550 to 625 nm. As shown in Figure S6, the strong blue fluorescence of blank MAL-PEG-Tripp micelles in the cytoplasm of cells in the donor channel (A1), no red fluorescence was observed in the FRET channel and acceptor channel because of the absence of red emitters (A2, A3). Interestingly, we found that the blue fluorescence from DOX-loaded MAL-PEG-Tripp micelles was slightly quenched (B1), meanwhile, the red fluorescence in the FRET channel (B2) and the acceptor channel (B3) were observed. These results suggested that the efficient FRET from the MAL-PEG-Tripp donor to the DOX acceptor was happened after the cellular internalization of DOX-loaded MAL-PEG-Tripp micelles. For the free DOX, however, there was no blue fluorescence was observed and the red fluorescence was only observed in the acceptor channel (C3).

The quantitative cellular uptake and drug release abilities of DOX-loaded MAL-PEG-Tripp micelles were further illustrated in flow cytometry. 4T1 breast cancer cells were used as a negative control and only autofluorescence of cells was observed. The free DOX and DOX-loaded MAL-PEG-Tripp micelles containing the same concentration DOX (10 μg/mL) were co-cultured with 4T1 cells for 1h and 3h. As presented in Figure 8A, the fluorescence intensity of DOX·HCl group was higher than that of DOX-loaded MAL-PEG-Tripp micelles group for 1 h incubation. The fluorescence intensities of both groups increased with longer incubation time, which suggested more DOX-loaded MAL-PEG-Tripp micelles accumulated in the cytosol. The result was in agreement with that of CLSM.

Moreover, the IC50 (half maximal inhibitory concentration) values of DOX·HCl (0.41μg/mL), DOX-loaded MAL-PEG-Tripp micelles (2.36 μg/mL) to 4T1 cells were investigated (Figure 8B). Compared to free DOX·HCl group, the lower anticancer activity of DOX-loaded MAL-PEG-Tripp micelles was owed to the slow release of DOX from micelles and the cellular uptake via endocytosis, which retarded the diffusion and aggregation of DOX from the cytoplasm to the nuclei. DOX·HCl was a water-soluble molecule, which diffused much faster into cells to kill cells efficiently and resulted in lower IC50.

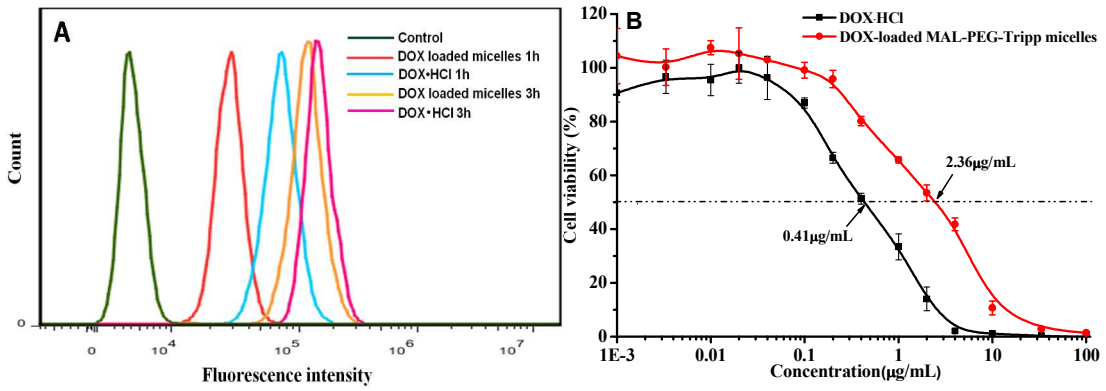

Figure 8. The flow cytometry histogram profiles of 4T1 cells incubated with DOX·HCl and DOX-loaded MAL-PEG-Tripp micelles for 1h and 3 h, the DOX concentration was 10 μg/mL (A); the IC50 of the DOX-loaded MAL-PEG-Tripp micelles against 4T1 cells, the incubation time was 48 h, means ± SD (n = 3) (B).

In vivo anticancer activity investigation

The in vivo anticancer activity study was carried out in breast cancer-bearing BALB/c mice. DOX·HCl (5 mg/kg) and DOX-loaded MAL-PEG-Tripp micelles (DOX, 5 mg/kg) were administrated via tail vein injection for 4 times and the saline was used as control. The changes of tumor sizes and body weight treated with DOX-loaded MAL-PEG-Tripp micelles, DOX·HCl and saline were presented in Figure 9.

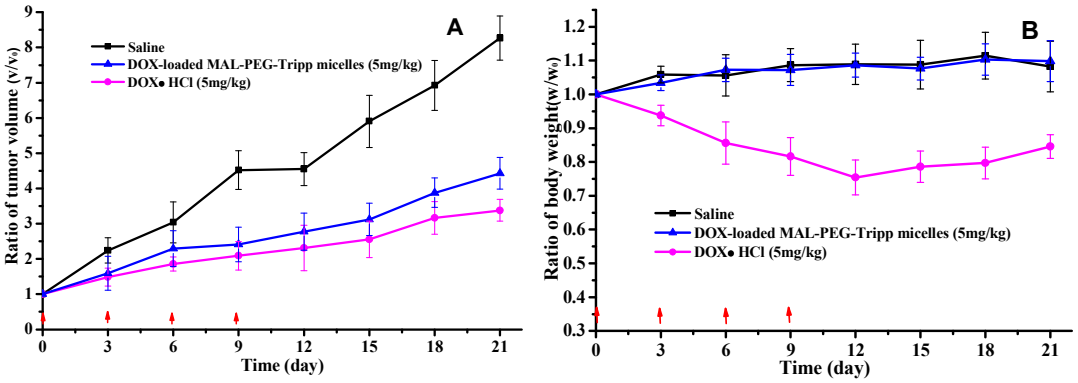

Figure 9. The in vivo anticancer activity of DOX-loaded micelles, (A) the volumes of tumors treated with DOX-loaded MAL-PEG-Tripp micelles, DOX·HCl and saline; p values at 21 days: DOX-loaded MAL-PEG-Tripp micelles, p=0.0062; DOX·HCl, p=0.0247, $P < 0.05$ meant significant difference; (B) body weights of the mice treated with DOX-loaded MAL-PEG-Tripp micelles, DOX·HCl and saline.

After 21days administration, the saline group showed almost no inhibition effect since the tumor volume increased rapidly. The DOX·HCl group exhibited the most efficient anticancer activity in vivo. And it is satisfied that the inhibition efficiency of the DOX-loaded MAL-PEG-Tripp micelles group was near to the free

DOX·HCl group (Figure 9A). The body weight of the mice treated with DOX·HCl decreased 20% after 12d. The mice not only suffered from substantial weight loss and weakness after injections, but also suffered from erythema on the mice, which indicated the severe systemic toxicity of DOX·HCl (Figure 9B). The body weight of the mice treated with DOX-loaded MAL-PEG-Tripp micelles did not show significant difference from that of saline group, which suggested DOX-loaded MAL-PEG-Tripp micelles did not exhibited marked side effect.

The histological tissues slides of tumor, heart, liver, spleen, lung and kidney of the tumor-bearing mice treated with DOX-loaded MAL-PEG-Tripp micelles, DOX·HCl, and saline were presented in Figure 10. The DOX-loaded MAL-PEG-Tripp micelles and DOX·HCl group exhibited much better tumor inhibition effect, as tumor necrosis with hemorrhage appeared in most areas. While the free DOX·HCl group led to serious heart toxicity as necrosis (heart image in DOX·HCl group) with acute inflammatory cells filtration in epicardium and congestion between myocardial cells. Simultaneously, little necrosis area in the center of neoplastic cells was observed in saline group (tumor image). White pulp atrophy and congestion occurred in spleen (spleen images). Lobular pneumonia was observed in lung in DOX·HCl and saline group, and less inflammation in micelles group. Kidney glomerular swelling shrinked or disappeared (kidney images in DOX·HCl and saline group). All the organs of heart, liver, spleen, lung and kidney in micellar formulation group were normal in the histological tissue slides, indicating less toxicity of micellar formulation to organs.

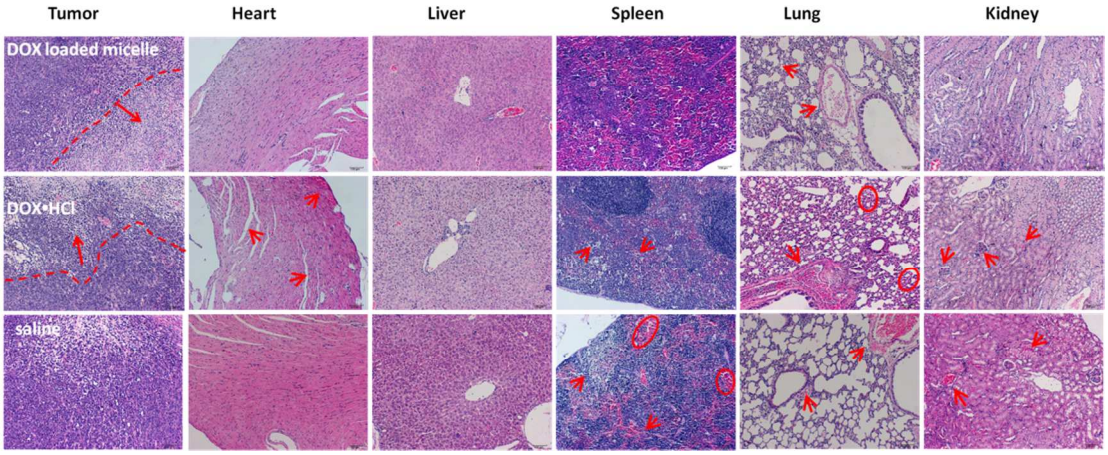

Figure 10. Histological analysis of different organs in tumor bearing mice with DOX-loaded MAL-PEG-Tripp micelles, DOX·HCl, and saline. Each group of BALB/c mice (male, n = 10) was intravenously administered four times at a three-day interval at a dose of 5 mg/kg (DOX).

Immunohistochemical analysis of CD31, Ki-67 and TUNEL

Invasion and metastasis always accompanied with angiogenesis in the process of solid tumors growth. The CD31 and Ki-67 antigen staining were further performed to assess the antitumor efficacy of DOX-loaded MAL-PEG-Tripp micelles on tumor cell proliferation, and the terminal deoxynucleotidyl transferase-mediated dUTP nick end labeling (TUNEL) assay was employed to detect apoptotic programmed cell death (Figure 11). About 47% of apoptotic cells were obtained for the DOX/MAL-PEG-Tripp micelles group and 54% for DOX·HCl group, both them were significantly different with the saline group (11%). The CD31 and Ki-67 immunohistochemical staining studies showed that the number of MVD and Ki-67-positive cells administrated with DOX·HCl actively inhibited the proliferation and induced the apoptosis of tumor cells.

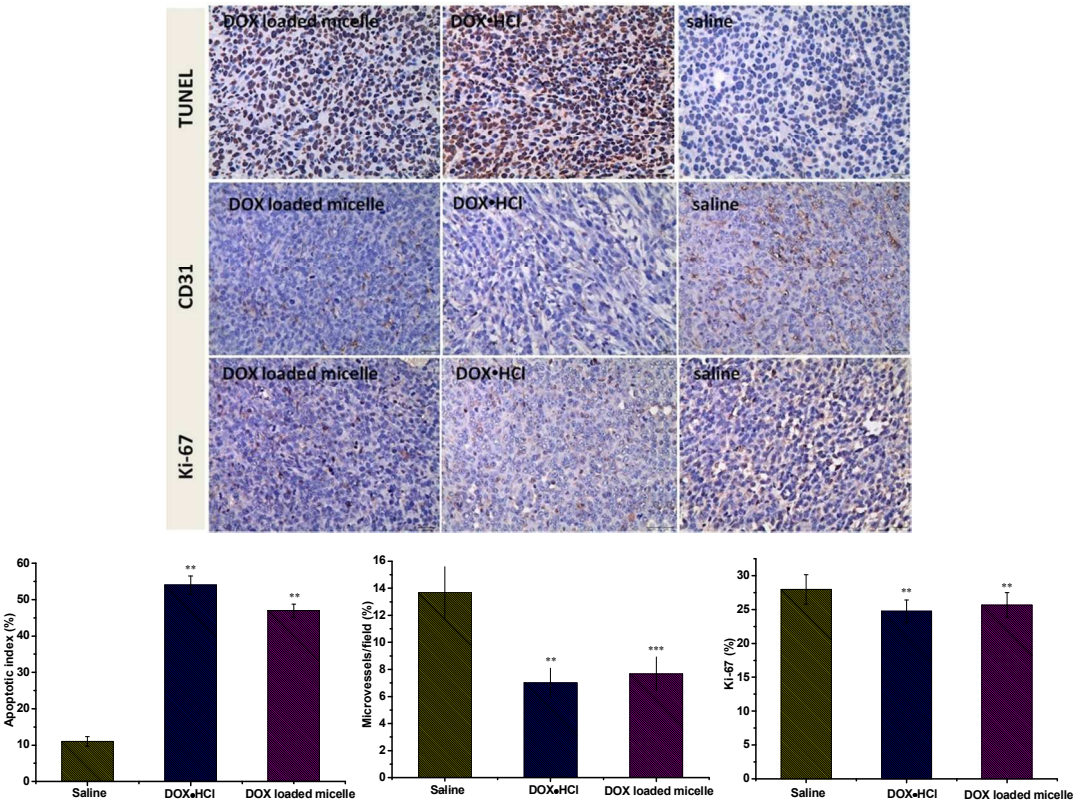

Figure 11. The TUNEL, Ki-67 and CD31 immunohistochemical (IHC) staining of tumor tissues (× 400). The brown areas indicated TUNEL-positive, CD31-positive or Ki-67 positive staining. The apoptotic index was calculated as the ratio of the apoptotic cell number to the total tumor cell number in each field of view. The CD31 positive area was expressed in endothelial cell pack and count capillary number by reading each section (MVD). The Ki-67 density in each image was calculated by Ki-67-positive area to total area. Data was presented as mean ± SD (n = 6) (*: P<0.05;**: P<0.01;***: P<0.001). The dose of DOX was 5 mg/kg.

CONCLUSION

This study devoted to obtain a polymeric micelle for cancer therapy with AIE effect for cell imaging and FRET for monitoring anticancer drug delivery. AIE molecule of Tripp-COOH was selected to fabricate the lyophobic micellar core for imaging, as well as generate FRET effect with doxorubicin (DOX) to detect the drug release. The results demonstrated this DOX-loaded MAL-PEG-Tripp micelle exhibited not only outstanding cellular tracing, but also excellent therapeutic efficacy and low side effects in cancer chemotherapy. This study provided an effective way to fabricate a polymeric micelle with the capacity for simultaneous cellular imaging, dynamic drug release monitoring, and chemotherapeutic treatment for effective therapy.

Materials and methods

Materials

Poly(ethylene glycol) (PEG, Mw = 2000g/mol), 1H-pyrrole-1-propanoicacid (MAL) and deuteron dimethyl sulphoxide (DMSO-d_6) were purchased from Sigma-Aldrich Co. Ltd. Phenylacetylene, methyl 4-aminobenzoate, 1-ethyl-(3-dimethyllaminopropyl) carbodiie hydrochlide (EDC·HCl) and 1-hydroxy-benzotriazole monohydrate (HOBt) were purchased from GL Biochem. Ltd. (Shanghai, China). Tetramethylethylenediamine, and *N*, *N*-diisopropylethylamine (DIEA) were purchased from Asta Tech Biopharm. Co. Ltd (Chengdu, China). Doxorubicin hydrochloride (DOX·HCl, Shanghai Yingxuan Chempharm Co. Ltd. China) was deprotonated according to the method previously reported.[31] Diethyl ether and CH_2Cl_2 were purified before use and all other solvents were used as received. All solvents were obtained from Chengdu Kelong Chemical Co. (China). Dulbecco's Modified Eagle's Medium (DMEM), Roswell Park Memorial Institute (RPMI) 1640 medium, fetal bovine serum (FBS), and cell counting kit-8 (CCK-8) were used for cytotoxicity test.

Characterizations

^{1}H NMR was performed on Bruker (400 MHz) in DMSO-d_6 with tetramethylsilane as the internal standard. The molecular weights were measured by matrix assisted laser desorption/ionization time-of-flight mass spectroscopy (MALDI-TOF-MS). The mean size and size distribution of the micelles were carried out using a dynamic light scattering (DLS) spectrometer (Malvern ZetasizerNano ZS). The morphology of the micelles was measured by transmission electron microscopy (TEM, JEM-100CX-JEOL). The samples were prepared by dropping the freshly micelle solution onto a copper grid coated with carbon film and dried overnight at room temperature before observation. The samples were negatively stained with 1% uranyl acetate aqueous solution. The AIE properties and FRET phenomenon were determined by UV-evisabsorption (Specord 200 PLUS) and Fluorescence spectra (HITACHI F-700).

Synthesis of MAL-PEG-Tripp

The synthetic process of the MAL-PEG-Tripp was presented in Scheme 1.

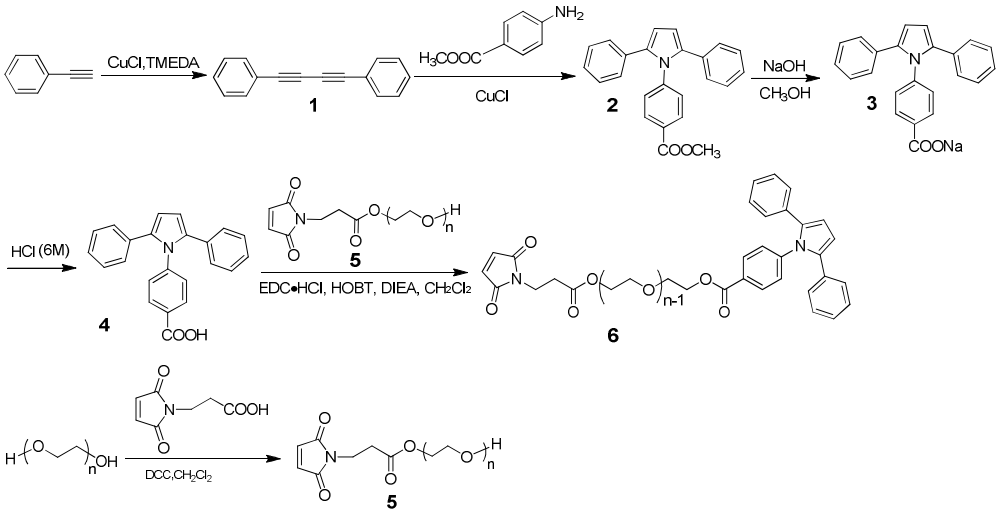

Scheme 1. The synthesis of MAL -PEG-Tripp.

Synthesis of Tripp-COOH

Compound **1** of 1, 4-diphenylbuta-1, 3-diyne was firstly synthesized according to the previous literature.[32] Then compound **1** (2.0 g, 1.0 mmol), copper (I) chloride (0.12 g, 1.0 mmol) and methyl 4-aminobenzoate (3.01 g, 20.0 mmol) were added to a 250 mL bottom-round flask stirred under argon atmosphere for 12 h at 115 °C. The crude product of compound **2** (Tripp-$COOCH_3$) was purified by silica column chromatography with the eluent (petroleum ether/dichloromethane = 2/1). Then the above purified product of compound **2** (0.28 g, 0.8 mmol) and NaOH (0.2 g, 5.0 mmol) were dissolved in 200 mL of methanol and stirred at 65 °C for 15 h, the crude product was precipitated in a large amount of CH_2Cl_2, the white solid precipitate was washed by acetone and chloroform for three times to obtain compound **3** (Tripp-COONa). Compound **3** was added to HCl (6 M) solution with stirring at room temperature for overnight and the product was washed by water several times to obtain compound **4** (Tripp-COOH).

Synthesis of MAL-PEG

PEG2k (10.0 g) and compound of MAL (1.0 g) were dissolved in 200 mL of the anhydrous CH_2Cl_2 in an ice bath under nitrogen atmosphere. A solution of DCC (2.06 g, 10.0 mmol) and DMAP (0.061 g, 0.5 mmol) in CH_2Cl_2 (60 mL) was added dropwise into the mixture. The mixture was stirred at room temperature for 48 h. The white solid dicyclohexylurea (DCU) precipitate was removed by filtration, the filtrate was concentrated and

precipitated into large amount of cold diethyl ether. This purification procedure was repeated for several times to obtain compound **5** (MAL-PEG).

Synthesis of MAL-PEG-Tripp

Compound **4** (0.41 g, 1.2 mmol), compound **5** (2.0 g, 1.0 mmol), EDC·HCl (0.27 g, 1.4 mmol) and HOBt (0.19 g, 1.4 mmol) were dissolved in anhydrous dichloromethane, DIEA was injected into this solution and stirred at room temperature for 48 h. The solution was concentrated by evaporated under vacuum and precipitated in a large amount of cold diethyl ether for three times. After that, the product was dialyzed with a molecular weight cutoff of 1000 Da and freeze-dried for further purification to obtain compound **6** (MAL-PEG-Tripp).

Critical micelle concentration (CMC)

A simple method was developed to determine the CMC by using the aggregation-induced emission of the amphiphiles, the emergence of the blue fluorescence of MAL-PEG-Tripp appeared when the formation of micelles in double distilled water. The solution with different concentration of MAL-PEG-Tripp (from 0.49 to 100 μg/mL) in double distilled water was processed by ultrasound for 0.5 h, the CMC of the amphiphiles was measured by fluorescence spectra. The fluorescence absorbance values at a wavelength of 480 nm were collected for the calculation of critical micelle concentration.

Preparation of drug-loaded micelles

Amphiphile (MAL-PEG-Tripp, 10 mg) and DOX (2.5 mg) were dissolved in 1 mL of DMSO. This mixture solution was sonicated for 1 h, and then dropped into 10 mL deionized water with vigorous stirring overnight. The solution was dialyzed against deionized water at 4 °C for 12 h in a dialysis tubing (Spectra/Por MWCO = 1000). The outer phase was replaced with fresh deionized water every 2 h. The solution in the tubing was lyophilized after centrifugation. The whole procedure was performed in the dark.

The content of encapsulated DOX was determined by UV-Vis measurement (λmax= 480 nm) in DMSO using calibration curve obtained from DOX/DMSO solutions with different DOX concentrations. Drug loading content (DLC) and drug loading efficiency (DLE) were calculated according to the following formulas:

DLC (%) = (weight of drug in micelle/weight of drug-loaded micelle)× 100%

DLE (%) = (weight of drug in micelle/weight of drug in feeding)× 100%

Drug release profile

DOX-loaded MAL-PEG-Tripp micelles were dispersed in PBS (1 mL, ionic strength = 0.01 M, pH = 7.4/5.5). The mixture was transferred into dialysis membrane tubing (Spectra/Por MWCO = 1000), the tubings were immersed in vials containing 25 mL of PBS solution. The vials were put in a shaking bed and the release profiles were tested at 37 °C. The volume of medium was kept constant by adding fresh medium after each sampling at

prescribed time intervals. The released DOX was detected by a fluorescence detector (λ_{ex}=480 nm, λ_{em}=550 nm). The release experiments were conducted in triplicate under sink conditions, the mean value was presented.

Cytotoxicity assessment

4T1 cells were cultured in RPMI 1640 media, C2C12 cells were cultured in DMEM medium. The media were supplemented with 10% fetal bovine serum and 1% penicillinstreptomycin at 37 °C in a humidified atmosphere with 5% CO_2. The cells were harvested with 0.02% EDTA and 0.025% trypsin and rinsed. The cytotoxicity of blank micelles was tested by 4T1 breast cancer cells and C2C12 cells. The cells were seeded in 96-well plates with 4×10^4 cells per well in 100 μL of medium for 24 h incubation before the tests. After 24 h incubation, the medium was removed and replaced with 100 μL of medium containing different concentrations of blank micelles. Then the cells were incubated for an extra 48 h. The culture medium was removed and the wells were rinsed with PBS (pH=7.4). 100 μL of Cell Counting Kit-8 assay (CCK-8, Dojindo, Japan, volume fraction 10%) solution was added to each well. After incubated for 2 h, the absorbance was measured in a Thermo Scientific MK3 (Thermo fisher; US) at the wavelength of 450 nm.

Cellular uptake

Confocal laser scanning microscopy (CLSM) and flow cytometry was employed to examine the cellular uptake of DOX·HCl and DOX-loaded MAL-PEG-Tripp micelles. 4T1 cells at a logarithm phase were seeded on 35 mm diameter glass dishes at a cell density of 1×10^4 mL^{-1}. After incubating for 24 h, DOX-loaded MAL-PEG-Tripp micelles were dissolved in each culture medium until the final DOX concentration was 10 μg mL^{-1}, The mixture was added into the each glass dishes with the medium removed. After incubated for 1 h and 3 h, the culture medium was removed and the dishes were rinsed with PBS (pH = 7.4). DOX was excited at 480 nm with emission at 590 nm.

For the flow cytometry tests, 4T1 cells were seeded in 6-well plates at a density of 2×10^5 mL^{-1} cells per well and incubated for 24 h. The cells were treated with DOX·HCl and s at the same DOX concentration (10 μg mL^{-1}) for 1 h and 3 h, respectively. The culture medium was eliminated, the cells were washed with PBS for three times and harvested by trypsinization. The cells were resuspended in PBS after centrifugation (1000 rpm, 5 min) and the fluorescence intensity was measured (λ_{ex}=480 nm; λ_{em}=590 nm) on a BD FACS Calibur flow cytometer (Beckton Dickinson).

In vitro anticancer activity

The anticancer activity of drug loaded micelles was evaluated in vitro with 4T1 cells. Cells were harvested and seeded in 96-well plates with 1×10^4 mL^{-1} cells per well with 100 μL medium for 24 h. DOX·HCl and DOX-loaded MAL-PEG-Tripp micelles in culture mediums were added to the plates with different DOX

concentrations (from 0.001 to 100 mg/mL) and incubated for 48 h. The cell viability was measured by CCK-8 assay.

In vivo antitumor activity study

All the animal experiments were performed according to the institutional and NIH guidelines for care and use of research animals. Male BALB/c mice (body weight: 21-24 g) were purchased from West China Experimental Animal Culture Center of Sichuan University. 5×10^5 4T1 cells were injected into right flank subcutaneously of BALB/c mice. The mice were randomly divided into 3 groups when the inoculated tumor volume reached about 100 mm^3, and then injected intravenously via the tail vein with a DOX dose of 5 mg/kg body weight for four times at a 3-day interval. The tumor volume and body weight were monitored at prescribed time intervals. The tumor volume was calculated by the flowing formula: $V(mm^3)=1/2\times ab^2$, where a and b presented the largest and smallest diameter of the tumor tissue respectively. All mice were sacrificed on day 21.

The heart, liver, spleen, lung, kidney and tumor were excised from each group and fixed in 4% formaldehyde for histological examination. The representative tissues were processed for routine histopathological procedures. Paraffin embedded specimens were cut into 5 mm sections and stained with hematoxylin and eosin (H&E) for histopathological evaluation.

Immunohistochemical analysis of CD31, Ki-67 and TUNEL

Streptavidine peroxidase methods were specially designed for Immunohistochemical (IHC) reactions and other immune detection. The paraffin-embedded tumor sections were deparaffinaged, rehydrated and incubated overnight at 4 °C with primary monoclonal antibody against CD31 or Ki-67(1:200) (British abcam-(Shanghai) trading Co., LTD). Biotinylated goat antirabbit antibodies were used as secondary antibodies at 1:200 for 30 min at room temperature and the egg protein reagent marked with horseradish peroxidase was added. The data of immunohistochemistry staining was obtained as described. IHC images were taken by the Motic Images Advanced software (Motic China Group CO., LTD.), the positive-stained integrated optical density (IOD) of the CD31 and ki-67 was scaled with each image by Image-Pro Plus 6.0 software (Media Cybernetics, Bethesda, MD). The microvessel density (MVD) was counted by reading each section which referenced Weidner method for quantitative analysis and the CD31 positive area was expressed in endothelial cell pack. In addition, the ki-67 density in each photograph was calculated as the ratio of ki-67-positive area to total area. For terminal deoxynucleotidyl transferase mediated UTP nick end labeling (TUNEL) assay, the dewaxed and rehydrated tumor tissue sections were incubated with proteinase K at 37 °C for 15 min, rinsed with PBS twice. The TUNEL assay was performed on in situ cell death detection kit-POD (Roche Group, Switzerland) to evaluate apoptotic cells. Positive TUNEL staining was visualized by optical microscopy and the apoptotic index was formulated as the ratio of apoptotic cell number to total tumor cell number in each microscope field.

Statistical analysis

All data are presented as means±S.D. Statistical significance ($p < 0.05$) was evaluated by using Student t-test when experiment groups were compared.

AUTHOR INFORMATION

Corresponding Author

W.X. Gao (wenxiag@wzu.edu.cn); L. Li (li_li@scu.edu.cn).

ACKNOWLEDGMENT

The authors thank for the financial support of National Science Foundation of China (No. 51573111, 21672164, 81371666), Program for Changjiang Scholars and Innovative Research Team in University (IRT-15R48), Ministry of Education of China (No. 20130181110038), and Natural Science Foundation of Zhejiang Province (LY15B020001).

SUPPORTING INFORMATION

Supporting information is available free of charge via the Internet at http://pubs.acs.org.

REFERENCES

(1) Shen, M., Huang, Y., Han, L., Qin, J., Fang, X., Wang, J., and Yang, V. C. (**2012**) Multifunctional drug delivery system for targeting tumor and its acidic microenvironment. *J. Control. Release. 161*, 884–892.

(2) Yu, M., Guo, F., Wang, J., Tan, F., and Li N. (**2016**) A pH-driven and photoresponsive nanocarrier: Remotely-controlled by near-infrared light for stepwise antitumor treatment. *Biomaterials. 79*, 25–35.

(3) Rong, P., Yang, K., Srivastan, A., Kiesewetter, D. O., Yue, X., Wang, F., Nie, L., Bhirde, A., Wang, Z., Liu, Z., et al. (**2014**) Photosensitizer loaded nano-graphene for multimodality imaging guided tumor photodynamic therapy. *Theranostics*. 4, 229–239.

(4) Li, Z., Zhang, Y., and Han, G. (**2013**) Lanthanide-doped upconverting luminescent nanoparticle platforms for optical imaging-guided drug delivery and therapy. *Adv. Drug Deliv. Rev. 65*, 744–55.

(5) Yuan, Y., Kwok, R., Zhang, R., Tang, B.-Z., and Liu, B. (**2014**) Targeted theranostic prodrugs based on an aggregation-induced emission (AIE) luminogen for real-time dual-drug tracking. *Chem. Commun. 50*, 11465–11468.

(6) Lin, R.Y., Dayananda, K., Chen, T.J., Chen, C.Y., Liu, G.C., Lin, K.L., and Wang, Y.M. (**2012**) Targeted RGD nanoparticles for highly sensitive in vivo integrin receptor imaging. *Contrast media & molecular imaging. 7*, 7–18.

(7) Couturier, L., Trylinski, M., Mazouni, K., Darnet, L., and Schweisguth, F. (**2014**) A fluorescent tagging approach in Drosophila reveals late endosomal trafficking of Notch and Sanpodo. *J. Cell Biol. 207*, 351–363.

(8) Bergson, S., Kalt, I., Itzhak, I., Brulois, K. F., Jung J. U., and Sarid, R. (**2014**) Fluorescent tagging and cellular distribution of the Kaposi's sarcoma-associated herpesvirus ORF45 tegument protein. *Journal of virology. 88*, 12839–12852.

(9) Marklein, R. A., Lo Surdo, J. L., Bellayr, I. H., Godil, S. A., Puri, R. K., and Bauer, S. R. (**2016**) High content imaging of early morphological signatures predicts long term mineralization capacity of human mesenchymal stem cells upon osteogenic induction. *Stem cells. 34*, 935–947.

(10) Peng, T., Chen, X., Gao, L., Zhang, T., Wang, W., Shen, J., and Yang, D. (**2016**) A rationally designed rhodamine-based fluorescent probe for molecular imaging of peroxynitrite in live cells and tissues. *Chem. Sci. 7*, 5407–5413.

(11) Ma, J., Wu, L., Hou, Z., Song, Y., Wang, L., and Jiang, W. (**2014**) Visualizing the endocytosis of phenylephrine in living cells by quantum dot-based tracking. *Biomaterials. 35,* 7042–7049.

(12) Wolfbeis, O.S. (**2015**) An overview of nanoparticles commonly used in fluorescent bioimaging. *Chem. Soc. Rev. 44*, 4743–4768.

(13) Kairdolf, B. A., Smith, A. M., Stokes, T. H., Wang, M. D., Young, A. N., and Nie, S. (**2013**) Semiconductor quantum dots for bioimaging and biodiagnostic applications. *Annual review of analytical chemistry. 6*, 143–162.

(14) Luo, P. G., Yang, F., Yang, S.-T. , Sonkar, S. K., Yang, L., Broglie, J. J., Liu, Y. and Sun, Y.-P. (**2014**) Carbon-based quantum dots for fluorescence imaging of cells and tissues. *RSC Advances. 4*, 10791–10807.

(15) Oh, E., Liu, R., Nel, A., Gemill, K. B., Bilal, M., Cohen, Y., and Medintz, I. L. (**2016**) Meta-analysis of cellular toxicity for cadmium-containing quantum dots. *Nature Nanotechnology. 11*, 479–486.

(16) Huang, M., Yu , R., Xu , K., Ye , S., Kuang , S., Zhu, X., and Wan, Y. (**2016**) An arch-bridge-type fluorophore for bridging the gap between aggregation-caused quenching (ACQ) and aggregation-induced emission (AIE). *Chem. Sci. 7*, 4485–4491.

(17) Yuan, W. Z., Lu, P., Chen, S., Lam, J. W. Y., Wang, Z., Liu, Y., Kwok, H. S., Ma, Y., and Tang, B.Z. (**2010**) Changing the behavior of chromophores from aggregation-caused quenching to aggregation-induced emission: development of highly efficient light emitters in the solid state. *Adv. Mater. 22*, 2159–2163.

(18) Luo, J., Xie, Z., Lam, J. W. Y., Cheng, L., Chen, H., Qiu, C., Kwok, H. S., Zhan, X., Liu, Y., Zhu, D., et al. (**2001**) Aggregation-induced emission of 1-methyl-1,2,3,4,5-pentaphenylsilole. *Chem. Commun. 18*, 1740–1741.

(19) Zuo, Y.-F., Wang, X., Yang, Y.-Y., Huang, D., Yang, F., Shen, H., and Wu, D.-C. (**2016**) Facile preparation of pH-responsive AIE-active POSS dendrimers for the detection of trivalent metal cations and acid gases. *Polymer Chemistry*. *7*, 6432-6436.

(20) Wang, X., Yang, Y. Y., Zhuang, Y. P., Gao, P. Y., Yang, F., Shen, H., Guo, H. X., and Wu, D. C. (**2016**) Fabrication of pH-responsive nanoparticles with an AIE feature for imaging intracellular drug delivery. *Biomacromolecules. 17*, 2920-2929.

(21) Yan, L., Zhang, Y., Xu, B., and Tian, W. (**2016**) Fluorescent nanoparticles based on AIE fluorogens for bioimaging. *Nanoscale. 8*, 2471–2487.

(22) Zhang, X., Zhang, X., Yang, B., Hui, J., Liu, M., Chi, Z., Liu, S., Xu, J., and Wei, Y. (**2014**) Facile preparation and cell imaging applications of fluorescent organic nanoparticles that combine AIE dye and ring-opening polymerization. *Polym. Chem. 5*, 318–322.

(23) Zhang, C., Jin, S., Li, S., Xue, X., Liu, J., Huang, Y., Jiang, Y., Chen, W. Q., Zou, G., and Liang, X. J. (**2014**) Imaging intracellular anticancer drug delivery by self-assembly micelles with aggregation-induced emission (AIE micelles). *ACS Appl Mater Interfaces. 6*, 5212–5220.

(24) Liow, S. S., Dou, Q., Kai, D., Li, Z., Sugiarto, S., Yu, C. Y. Y., Kwok, R. T. K., Chen, X., Wu, Y. L., Ong, S. T., et al. (**2017**) Long-term real-time in vivo drug release monitoring with AIE thermogelling polymer. *Small. 13*, 1603404.

(25) Situ, B., Chen, S., Zhao, E., Leung, C. W. T., Chen, Y., Hong, Y., Lam, J. W. Y., Wen, Z., Liu, W., Zhang, W., et al. (**2016**) Real-time imaging of cell behaviors in living organisms by a mitochondria-targeting AIE fluorogen. *Adv. Funct. Mater.* 26, 7132–7138.

(26) Yan, L., Zhang, Y., Xu, B., and Tian, W. (**2016**) Fluorescent nanoparticles based on AIE fluorogens for bioimaging. *Nanoscale. 8*, 2471–2487.

(27) Xue, X., Zhao, Y., Dai, L., Zhang, X., Hao, X., Zhang, C., Huo, S., Liu, J., Liu, C., Kumar, A., et al. (**2014**) Spatiotemporal drug release visualized through a drug delivery system with tunable aggregation−induced emission. *Adv Mater. 26*, 712–727.

(28) Yuan, Y., and Liu, B. (**2017**) Visualization of drug delivery processes using AIE gens. *Chem. Sci. 8,* 2537–2546.

(29) Zuo, Y. F., Wang, X., Yang, Y. Y., Yang, F., Shen, H., and Wu, D. C. (**2016**) Facile creation of FRET systems from a pH-responsive AIE fluorescent vesicle. *Chem. Commun. 52*, 5320-5323.

(30) Feng, L., Li, K., Shi, X., Gao, M., Liu, J., and Liu, Z. (**2014**). Smart pH-responsive nanocarriers based on nano-graphene oxide for combined chemo- and photothermal therapy overcoming drug resistance. *Adv. Healthcare Mater. 3*, 1261–1271.

(31) Shuai, X., Ai, H., Nasongkla, N., Kim, S., and Gao, J. (**2004**) Micellar carriers based on block copolymers of poly(ε-caprolactone) and poly(ethylene glycol) for doxorubicin delivery. *J Controlled Release. 98*, 415–426.

(32) Hay, A. S. (**1962**) Oxidative coupling of acetylenes. II[1]. *J. Org. Chem. 27*, 3320–3321.

Table of Contents (TOC)